

This is a copy of the published version, or version of record, available on the publisher's website. This version does not track changes, errata, or withdrawals on the publisher's site.

Spin dynamics, entanglement, and the nature of the spin liquid state in YbZnGaO₄

F. L. Pratt, F. Lang, W. Steinhardt, S. Haravifard, and S. J. Blundell


Published version information

Citation: FL Pratt et al. Spin dynamics, entanglement, and the nature of the spin liquid state in YbZnGaO₄. Phys Rev B 106, no. 6 (2022): L060401

DOI: [10.1103/PhysRevB.106.L060401](https://doi.org/10.1103/PhysRevB.106.L060401)

This version is made available in accordance with publisher policies. Please cite only the published version using the reference above. This is the citation assigned by the publisher at the time of issuing the APV. Please check the publisher's website for any updates.

This item was retrieved from **ePubs**, the Open Access archive of the Science and Technology Facilities Council, UK. Please contact epublications@stfc.ac.uk or go to <http://epubs.stfc.ac.uk/> for further information and policies.

Spin dynamics, entanglement, and the nature of the spin liquid state in YbZnGaO₄F. L. Pratt^{1,*}, F. Lang¹, W. Steinhardt,² S. Haravifard², and S. J. Blundell³¹*ISIS Neutron and Muon Source, STFC Rutherford Appleton Laboratory, Chilton, Didcot OX11 0QX, United Kingdom*²*Department of Physics, Duke University, Durham, North Carolina 27708, USA*³*Department of Physics, University of Oxford, Clarendon Laboratory, Oxford OX1 3PU, United Kingdom* (Received 23 November 2021; revised 18 June 2022; accepted 20 July 2022; published 1 August 2022)

Electron spin dynamics was studied down to 80 mK in the triangular-lattice quantum spin-liquid candidate YbZnGaO₄ using muon spin relaxation, finding no evidence for freezing or ordering of the Yb spins. The muon spin relaxation rate can be represented by the sum of two contributions, one dependent on longitudinal magnetic field and the other independent of field. The field-dependent term follows the form expected for two-dimensional diffusion of mobile spin excitations. The spin-diffusion rate obtained for these excitations in the high temperature paramagnetic regime is comparable with the exchange coupling frequency J/h , reducing significantly in the low temperature quantum regime. This slowdown is assigned to the effect of quantum entanglement. The exchange coupling J is estimated to be 2.0(2) K from the crossover between the two regimes. The field-independent term is only weakly dependent on temperature, and at 15 K its absolute value is consistent with dipolar coupling of the muon to the three Yb moments closest to the muon site, where the spin dynamics of these moments is determined by exchange fluctuations. The temperature-dependent properties in the quantum regime are compared against the three possible U(1) spin-liquid models that have been obtained for the strongly spin-orbit coupled triangular lattice by Y.-D. Li, Y.-M. Lu, and G. Chen [Phys. Rev. B **96**, 054445 (2017)]. The comparison with theory takes published specific heat and thermal conductivity data into account, along with the spin-diffusion rate obtained from the muons. It is found that the nodal spin-liquid model U1A11 containing both linear and quadratic nodes provides better agreement with experiment than either the U1A00 spinon Fermi surface (FS) model or the U1A01 model that contains only linear nodes.

DOI: [10.1103/PhysRevB.106.L060401](https://doi.org/10.1103/PhysRevB.106.L060401)

A quantum spin liquid (QSL) is a ground state for an antiferromagnetic system that is characterized by a high degree of quantum entanglement and fractionalized excitations [1,2]. Originally proposed for spin-1/2 Heisenberg systems on a triangular lattice [3], QSL states are found in triangular lattice models with interactions beyond nearest neighbor, and these can also include models with strong spin-orbit interactions.

YbMgGaO₄ (YMGO) and YbZnGaO₄ (YZGO) are a pair of triangular-lattice antiferromagnets that are members of a family that have attracted considerable attention in the past as they show both geometrical and site-disorder frustration [4]. They contain spatially well-isolated quasi-2D layers of Yb³⁺ (4*f*¹³) ions, which experience strong spin-orbit coupling. YMGO was proposed as the first candidate for a QSL with strong spin-orbit coupling and an odd number of electrons per unit cell. The spin is described by a Kramers doublet ground state, and a large crystal electric field gap of $\Delta \sim 420$ K separates it from excited doublets. Only the ground state Kramers doublet is active at temperatures below Δ , giving an effective spin-1/2 local moment [5,6].

Magnetic properties of YMGO have been characterized using various techniques [5,6]. The magnetic heat capacity shows $C_m \sim T^{0.7}$ behavior and the magnetic susceptibility remains constant in the zero temperature limit, indicating

an absence of magnetic order down to 60 mK [5,6], while the antiferromagnetic coupling is confirmed by the negative Weiss temperature ($\theta_W = -4.11$ K). Recent μ SR measurements also confirm that the system remains disordered down to 50 mK [7], now extended down to 22 mK [8].

Reported inelastic neutron-scattering experiments for YMGO [9,10] reveal a broad diffusive magnetic excitation continuum covering a wide region of the Brillouin zone with a weak diffuse peak at the M -symmetry points. In one study, a U(1) QSL with a spinon FS was suggested to represent the data [9]. Another study suggested that the XXZ exchange interaction on both nearest-neighbor and next-nearest-neighbor accounts for the spin-wave dispersion reported in magnetic fields and the diffuse peak at the M -points [10].

Fifty-fifty site mixing between the nonmagnetic Mg²⁺ and Ga³⁺ cations is an important feature of YMGO (and YZGO), and recent theoretical calculations have suggested that the ground state of YMGO is in fact a magnetically ordered stripe state [11] which is particularly fragile towards orientational disorder. It was thus proposed that the inhomogeneous charge environment from the Mg/Ga site mixing results in mimicry of a spin-liquid state in the form of short-range stripe or stripe superposition domains. However, previous μ SR studies of YMGO [7,8,12] as well as the present study of YZGO find no evidence for such a mimic state.

Other theoretical work has discussed the role of chemical disorder as well as the spin-orbit coupling in driving YMGO

*francis.pratt@stfc.ac.uk

towards a nodal QSL state rather than a FS state [13]. Three U(1) QSL states were found in a theoretical study of the spin-orbit coupled triangular lattice model: one state with a large FS and two symmetry-protected nodal states [14]. Another study put forward the argument that both YMGO and YZGO have a spin-glass ground state [15] on the basis of AC susceptibility and preliminary zero-field neutron-scattering measurements performed on YZGO. However, μ SR finds no evidence of glassy behavior down to as low as 22 mK in YMGO [7,8,12]. Magnetization measurements for YMGO taken down to 40 mK [16] also exclude the possibility that the low-temperature state includes a significant fraction of frozen spins. In the present study of YZGO we find no evidence for spin freezing in measurements taken down to 80 mK.

We measure here the YZGO system using μ SR [17] in both zero field (ZF) and longitudinal field (LF) configurations. ZF is used to confirm the absence of any spin freezing or magnetic ordering and LF is used to study the spin dynamics, making use of the dependence of the muon spin relaxation rate on the fluctuations of the local magnetic field at the muon site. Our sample was characterized to be phase pure via single crystal x-ray diffraction [18]. Weiss constants obtained from the magnetic susceptibility for field oriented with respect to the c axis were $\theta_{\parallel} = -2.67$ K and $\theta_{\perp} = -2.62$ K [18]. The corresponding J value is 1.76 K, weaker than $J \sim 2.8$ K obtained in the same way for YMGO [9,15]. The exchange anisotropy is lower than for YMGO, just on the Ising side of the Heisenberg limit. This contrasts with the XY side for YMGO [18].

We find that a diffusive model of spin dynamics provides a very good description of our μ SR data on YZGO. Diffusive models for spin dynamics have previously been used in μ SR and NMR investigations of quantum magnets, including spin chains [19–22] and spin liquids [23]. Theoretical work has focused mainly on 1D systems and the XXZ model, where diffusive spin transport is expected for exchange anisotropy on the Ising side of the Heisenberg point [24]. This corresponds to the exchange anisotropy of YZGO. With XY anisotropy, the transport has been suggested to switch over to ballistic character [25], and examples of ballistic spin dynamics have also been identified in μ SR studies of spin chain systems [26,27].

For the LF- μ SR studies a powder sample (prepared as reported previously [18]) was cooled in a dilution refrigerator giving temperatures down to 80 mK. After removing the mixture, the same cryostat could be used to extend the measurements up to 185 K, which allowed us to probe the effect of thermally populating crystal-field excitations. The EMU spectrometer at the ISIS Facility was used to collect $\sim 4 \times 10^7$ muon decay events per data point [28]. The maximum available field was 450 mT. The forward to backward asymmetry of the muon decay positrons $a(t)$ was fitted to a single relaxation component, consistent with a single muon site [29], i.e.,

$$a(t) = a_{\text{rel}}P_z(t) + a_{\text{bg}}, \quad (1)$$

where $P_z(t)$ is a stretched exponential function

$$P_z(t) = \exp(-(\lambda t)^{\beta}) \quad (2)$$

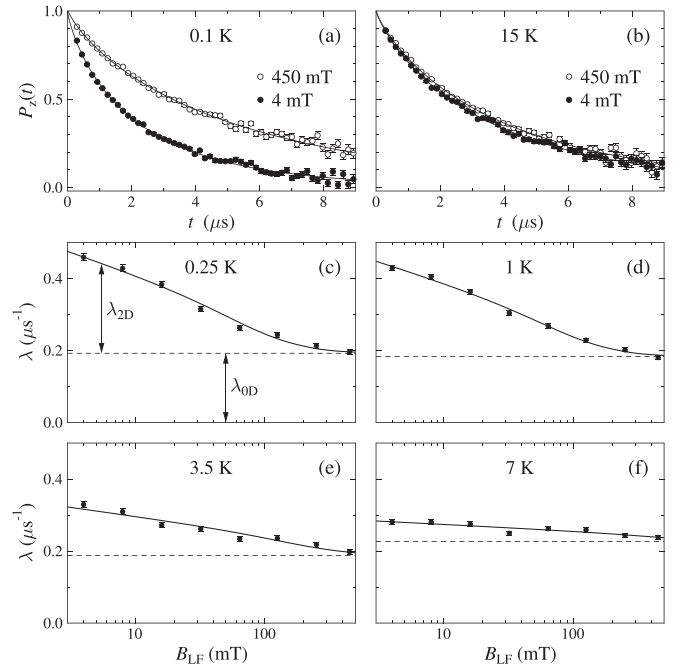


FIG. 1. Examples of normalized background-subtracted LF μ SR relaxation data for YZGO at (a) 0.1 K and (b) 15 K. Solid lines are fits to Eq. (1). A common β value is used for each T (ranging from 0.79 to 0.86) [30]. (c) to (f) show λ versus B_{LF} with fits to Eq. (3) shown as solid lines.

with λ the muon spin relaxation rate [30]. Some example LF- μ SR relaxation data are shown in Fig. 1, comparing data for temperature T well below J at 0.1 K [Fig. 1(a)] with data well above J at 15 K [Fig. 1(b)]. Significant relaxation remains present at 450 mT for both temperatures and a sizable increase of relaxation rate is seen on reducing the field to 4 mT for the low T case. The LF dependence of λ is shown in more detail in Figs. 1(c)–1(f) [31]. It can be represented by the sum of two terms: a field-dependent term $\lambda_{2\text{D}}$ representing diffusive spin excitations within the 2D planes, and a field-independent term $\lambda_{0\text{D}}$ representing rapidly fluctuating localized spin excitations

$$\lambda(B_{\text{LF}}) = \lambda_{2\text{D}}(B_{\text{LF}}) + \lambda_{0\text{D}}. \quad (3)$$

The $\lambda_{0\text{D}}$ term is consistent with dipolar coupling to spins that are fluctuating at the fast rate $\nu_{0\text{D}} > \gamma_{\mu}B_{\text{LF}}$, giving $\lambda_{0\text{D}} \propto \nu_{0\text{D}}^{-1}$ [29]. The 2D term reflects the spectral density of spin fluctuations at the probe frequency $\omega \propto B_{\text{LF}}$, i.e.,

$$\lambda_{2\text{D}}(B_{\text{LF}}) = \frac{C^2}{4} J_{2\text{D}}(\omega), \quad (4)$$

where C is a coupling parameter that includes contact and dipolar contributions [29,32]. Due to the presence of the contact hyperfine coupling, we have $\omega = \gamma_e B_{\text{LF}}$ [29]. In Eq. (4), $J_{2\text{D}}$ is the spectral density for a 2D random walk given by the Fourier transform of $S_{2\text{D}}$, the autocorrelation function for the 2D motion, given by [33]

$$S_{2\text{D}}(t) = [\exp(-2D_{2\text{D}}t)I_0(2D_{2\text{D}}t)]^2, \quad (5)$$

where $D_{2\text{D}}$ is the diffusion rate and I_0 is a zero order modified Bessel function of the first kind. $S_{2\text{D}}(t)$ notably follows a t^{-1} power law at long t .

TABLE I. Coupling parameter C and exchange parameter J obtained from fitting the complete LF data set.

C (MHz)	J (K)	J/h (ns $^{-1}$)
67(2)	2.0(2)	42(4)

A fit of the LF dependence of λ at 14 different temperatures between 0.1 K and 15 K was made with C as a global T -independent parameter (Table I), fitting individual D_{2D} and λ_{0D} values for each T scan. Examples of these fits are shown as the solid lines in Figs. 1(c)–1(f) [31].

For comparison, we also tried fitting to a simple fluctuation model, whose spectral density for fluctuation rate ν is given by $J_\nu(\omega) = 2\nu/(\nu^2 + \omega^2)$. This however gave a global fit that was 2.5 times worse than the 2D diffusion model. The reason for this is that the simple fluctuation model has a sharp cutoff which does not properly describe the slow variation with field in our data. This slow field variation implies a broad distribution of relaxation times, which is an intrinsic property of a random-walk diffusion process. We also compared the 2D diffusion model with previously reported LF- μ SR data for YMGO [7]. From this analysis we found that our 2D spin-diffusion model provides a better fit to YMGO than any of the previously considered models [34].

The fitted diffusion rate D_{2D} shows contrasting behavior for different T regions [Fig. 2(a)]. In the classical region ($T \gg J$) D_{2D} increases with T and its absolute value is comparable with J/h at the two highest measured T points. In contrast, for the quantum regime ($T \ll J$) D_{2D} is strongly suppressed

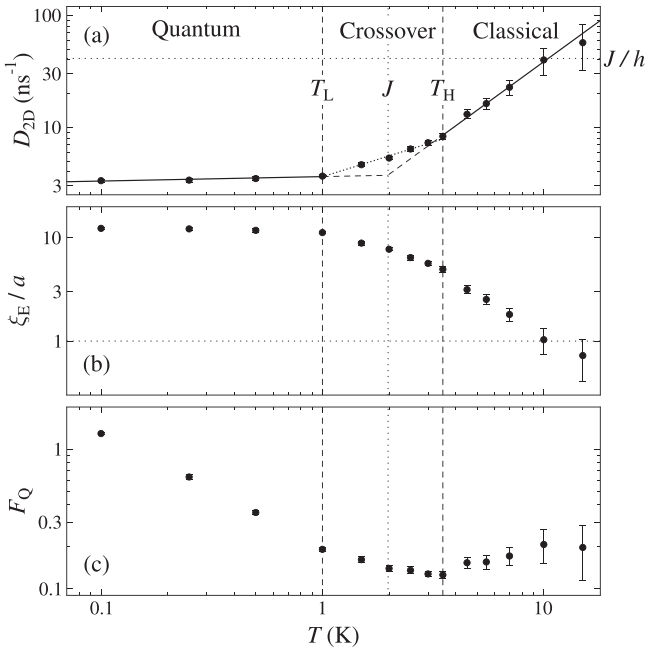


FIG. 2. (a) The 2D spin diffusion rate showing crossover between quantum and classical regimes around $J = 2.0$ (2) K. The 10 K and 15 K points are consistent with the inverse time scale defined by J/h (horizontal dotted line). (b) the quantum entanglement length ξ_E obtained from Eq. (8). (c) the F_Q values derived by applying Eq. (9) to the fitted J_{2D} .

 TABLE II. Representation of D_{2D} by T^{n_D} power laws. Regional boundaries are $T_L = 1$ K and $T_H = 3.5$ K.

D_{2D} at T_L (ns $^{-1}$)	n_D	Region
3.6(1)	0.04(2)	$(0.1 \text{ K} < T < T_L)$
	0.62(4)	$(T_L < T < T_H)$
	1.4(2)	$(T_H < T < 15 \text{ K})$

compared to J/h and the T dependence is very weak. In between these two regions there is a crossover region where T is comparable to J . The data can be well represented by T^{n_D} power laws in the three regions (Table II). An estimate for J can be obtained from the intersection of the extrapolated low and high T fits. This J (Table I) is fully consistent with the value obtained from the susceptibility.

The field-independent component λ_{0D} (Fig. 3) reflects a localized electronic relaxation mechanism. In the paramagnetic region the expected exchange fluctuation rate with $z = 6$ neighbors is [35] $\nu_{\text{ex}} = J/h\sqrt{2zS(S+1)/3} = 7 \times 10^{10} \text{ s}^{-1}$. When including dipolar couplings D_i between the muon and its three nearest Yb ions [29] (muon sites were calculated using the CASTEP Density Functional Theory code [36] with the PBE functional [37]), we estimate ν_{0D} from $2/\lambda_{0D} \sum_i D_i^2$ to be $5 \times 10^{10} \text{ s}^{-1}$ at 15 K, i.e., comparable to ν_{ex} . A high-field cutoff for λ_{0D} is predicted at $\nu_{0D}/\gamma_\mu = 56$ T, consistent with the absence of field dependence in λ_{0D} up to 0.45 T. Above 10 K we find that λ_{0D} is dominant at all fields, as seen by comparison with λ_{ZF} (Fig. 3). A rapid fall of λ_{ZF} above 100 K indicates a sharp increase in fluctuation rate. We fit to an activation curve of the form $\lambda_{ZF}^{-1} = \nu_0 + \nu_1 \exp(E_A/T)$, where ν_0 is given a weak power law T dependence for the best fit (Fig. 3, dashed line). This yields an activation energy $E_A = 3.9(4) \times 10^2 \text{ K}$, which is comparable to the value $\Delta = 423(1) \text{ K}$ deduced for the lowest crystal field excitation of Yb^{3+} in YMGO from specific heat [5].

We now consider the origin of the significant reduction in D_{2D} for the quantum regime. The diffusion rate D_{2D} is related to the diffusion constant D , the mean particle velocity v , the

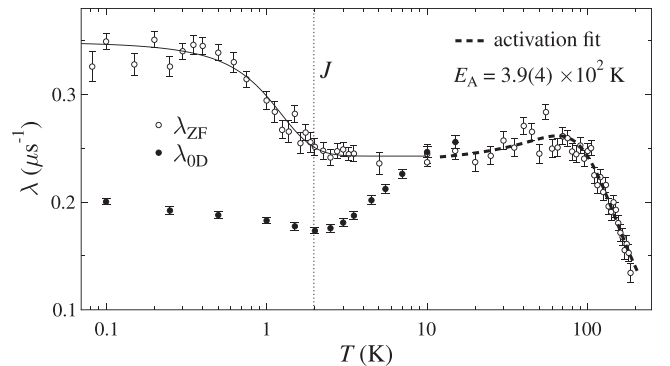


FIG. 3. The ZF relaxation rate and localized relaxation rate λ_{0D} . The solid line is a guide to the eye. The rise in λ_{ZF} when T falls below J mirrors the increase in λ_{2D} . At high T there is a sharp fall in λ_{ZF} above 100 K, reflecting a rapidly increasing electronic fluctuation rate due to crystal field excitations. The fitted activation energy E_A is indicated.

TABLE III. Characteristic parameters and expected thermal power laws for different types of spinon dispersion compared with experimental results for YZGO. Experimental values for n_κ and n_C are from the data of Ma *et al.* [15]. The last three columns list the three possible U(1) QSL states found by Li *et al.* [14] for a triangular-lattice QSL with strong spin-orbit coupling. Asterisks in these columns indicate the presence of that particular type of low energy spinon dispersion. Of these three states, only the U1A11 QSL provides the combination of linear and quadratic nodal contributions that match well with experiment.

	m	q	n_v	n_D	n_κ	n_C	U1A00	U1A01	U1A11
Fermi Surface (bare)		0	0	0	1	1	*		
with fluctuations (clean limit)				1/3	1/3	2/3			
with fluctuations (disordered limit)				-1/3	1	2/3			
Nodal									
Linear node	1	1	0	0	2	2		*	*
Quadratic node	2	0	0.5	0.5	1.5	1			*
Experiment				0.04(2)	~ 2	0.59(2)			

momentum relaxation time τ , and the mean free path $l = v\tau$ via [38]

$$D = \frac{1}{2}v^2\tau = \frac{1}{2}vl = D_{2D}l^2, \quad (6)$$

so that

$$D_{2D} = \frac{v}{2l}. \quad (7)$$

In the high T region the velocity is the product of the site separation $a = 3.412 \text{ \AA}$ and the transit rate for the pair exchange dynamics $2J/h$. Saturation of l at a gives the asymptotic value $D_{2D} = J/h$, consistent with the higher T points [Fig. 2(a)]. If v is independent of T on cooling, e.g., as would be the case for a spinon FS, then the reduction seen in D_{2D} at low T can be taken to reflect an increase in l . The low T value of D_{2D} indicates that l becomes saturated to $\sim 12a$. This defect scattering length scale is notably larger than that of the local Ga/Zn site disorder.

An alternative view of the large l in the quantum region would be that it represents a quantum entanglement length ξ_E [39], which decreases significantly on warming as T becomes comparable to J and the entanglement of the spins is strongly reduced compared to the entanglement at low T . Figure 2(b) shows the corresponding T dependence of ξ_E (which is equivalent to l) derived as

$$\frac{\xi_E}{a} = \frac{J}{h} \frac{1}{D_{2D}}. \quad (8)$$

The increase of ξ_E in the quantum region can be compared to the entanglement increase that could be obtained using a measure such as the quantum Fisher information entanglement witness F_Q [40,41], given here by the weighted integral of the spectral density

$$F_Q = \frac{4}{\pi} \int_0^\infty \tanh^2\left(\frac{\hbar\omega}{2k_B T}\right) J(\omega) d\omega, \quad (9)$$

which is shown in Fig. 2(c) for the J_{2D} term. Although the ξ_E and F_Q entanglement parameters both increase significantly on going between the classical and quantum regions, they evolve differently with T . The ξ_E value starts rising when T falls below 10 K and then saturates below 1 K. In contrast, F_Q only starts to rise significantly when T is below J . This difference in T dependence may reflect a difference in sensitivity to

local and nonlocal entanglement, since it has been suggested that F_Q should be blind to nonlocal entanglement [40].

Turning next to the more detailed nature of the QSL state, we note that the spinon specific heat for the FS model is predicted to have a thermal power law T^{n_C} with $n_C = 1$, which is broadly consistent with experiment (Table III). The magnetic thermal conductivity follows the product of the spinon specific heat and the diffusion constant, i.e., $\kappa \propto C_m v l$, which determines its power law n_κ . A significant problem with the FS model is that it predicts $n_\kappa = 1$, which has not been observed in either YZGO [15] or YMGO [42], where the observed power law for the total thermal conductivity is approximately quadratic and the effect of magnetic field on κ [15] suggests that both the spinon and the phonon contributions have a form that is close to quadratic.

Gauge fluctuations can modify the thermal power laws, and this effect has been worked out for the case of the spinon FS [43]. A reduction of n_C to 2/3 was predicted, which is very close to experiment. The corresponding correction for thermal conductivity in the clean limit would reduce n_κ to 1/3. However, in the limit of a disorder-related mean free path, which we take to apply here, n_κ remains at 1. Hence, the absence of a low n_κ term in the measured thermal conductivity [15,42] remains a serious challenge for a FS model in either limit. The corresponding corrected n_D values in the clean and dirty limits are given by $n_\kappa - n_C$ as 1/3 and -1/3, both deviating significantly from experiment (Table III).

In addition to the FS state, nodal states of the linear (Dirac) and quadratic band touching type are in general possible, and these can produce different power laws compared to the FS case (Table III). A dispersion of the excitations of the form $E \propto k^m$ may produce additional T dependence via the E dependence of the density of states (DOS) and the velocity. For a nodal 2D system the DOS follows E^q where $q = 2/m - 1$ and v follows $E^{(m-1)/m}$. For linear dispersion $q = 1$ and v is constant, whereas a quadratic band has $q = 0$ and a v^2 that is linear in T ($n_v = 0.5$). In the absence of fluctuations we expect $n_C = 1 + q$ and $n_D = n_v$. Since the diffusion rate is proportional to the diffusion constant in the quantum regime where l is saturated, we also expect the relation $n_\kappa = n_C + n_D$ to apply in this low T regime.

Table III compares parameters between different types of QSL models and experiment. Both the bare FS model and the linear node model predict $n_D = 0$, which is consistent with

our LF- μ SR data. However, the additional DOS factor from $q = 1$ in the linear node predicts that both n_κ and n_C become two, which is consistent with experiment for n_κ , but not for n_C . On the other hand, a quadratic nodal state has $n_C = 1$ (closer to experiment), but $n_D = 0.5$ and $n_\kappa = 1.5$ (both further from experiment).

As noted earlier, three possible U(1) QSL states were found for the strongly spin-orbit coupled triangular-lattice QSL by Li *et al.* [14]. The FS state has projective symmetry group label U1A00 and the second state U1A01 has linear nodes. The third U1A11 state uniquely contains both linear Dirac cones at the M points and quadratic touching bands at the Γ point [14]. For this U1A11 state the discrepancies with experiment can be resolved, since the high velocity linear regions will dominate transport, giving $n_D = 0$ and $n_\kappa = 2$, whereas the large DOS quadratic region will dominate specific heat, giving $n_C = 1$. This predicted n_C value is still larger than that observed, but it might plausibly be reduced from 1 to 2/3 by fluctuations, as found for the FS case, which would then give an even better match with experiment. Thus we conclude that only the nodal U1A11 QSL can simultaneously be consistent with the experimental values of n_D , n_κ , and n_C .

One question to consider is whether such a nodal state is compatible with the inelastic neutron scattering measured for YMGO [9,10] and YGZO [15,18]. Due to the low energy scale set by J , the neutron measurements do not probe low enough energies here to clearly distinguish between U1A00 and U1A11 states. In this situation the thermal and transport properties addressed in the present paper are particularly valu-

able for providing the crucial information on the low energy excitations. In particular, we make note that the absence of a thermal conductivity term with n_κ value of 1 or 1/3 in a QSL can point towards the presence of a nodal region in the spinon dispersion. A nodal magnetic contribution to the thermal conductivity following T^2 would always be hard to separate reliably from the phonon contribution, which typically also follows T^2 at low temperatures. Such a nodal contribution might also resolve the recent controversy about the thermal conductivity in another triangular lattice QSL, $\text{EtMe}_3\text{Sb}[\text{Pd}(\text{dmit})_2]_2$ [44–48].

Lastly, we note that there are many possible Z_2 QSL states in addition to the U(1) QSL states that might provide the ground state, as pointed out previously [13]. However, unlike the U(1) states, these Z_2 states have not yet been examined in detail, so we leave open the possibility that the nodal QSL ground state found here is actually a nodal Z_2 state [49], as was recently suggested for the triangular-lattice system 1T-TaS₂ [23]. Such a state can be viewed as resulting from a spinon pairing instability of an underlying FS state.

We are thankful to Casey Marjerrison for discussions and her help with this project in its early stages. The work at Duke University has been supported by William M. Fairbank Chair in Physics and NSF under Grant No. DMR-1828348. We acknowledge support from EPSRC (Grant No. EP/N023803/1). Part of this work was carried out at the ISIS Neutron and Muon Source, STFC Rutherford Appleton Laboratory, U.K.

-
- [1] Y. Zhou, K. Kanoda, and T.-K. Ng, *Rev. Mod. Phys.* **89**, 025003 (2017).
- [2] L. Savary and L. Balents, *Rep. Prog. Phys.* **80**, 016502 (2017).
- [3] P. W. Anderson, *Mater. Res. Bull.* **8**, 153 (1973).
- [4] R. J. Cava, A. P. Ramirez, Q. Huang, and J. J. Krajewski, *J. Solid State Chem.* **140**, 337 (1998).
- [5] Y. Li, G. Chen, W. Tong, L. Pi, J. Liu, Z. Yang, X. Wang, and Q. Zhang, *Phys. Rev. Lett.* **115**, 167203 (2015).
- [6] Y. Li, H. Liao, Z. Zhang, S. Li, F. Jin, L. Ling, L. Zhang, Y. Zou, L. Pi, Z. Yang, J. Wang, Z. Wu, and Q. Zhang, *Sci. Rep.* **5**, 16419 (2015).
- [7] Y. Li, D. Adroja, P. K. Biswas, P. J. Baker, Q. Zhang, J. Liu, A. A. Tsirlin, P. Gegenwart, and Q. Zhang, *Phys. Rev. Lett.* **117**, 097201 (2016).
- [8] Z. Ding, Z. Zhu, J. Zhang, C. Tan, Y. Yang, D. E. MacLaughlin, and L. Shu, *Phys. Rev. B* **102**, 014428 (2020).
- [9] Y. Shen, Y.-D. Li, H. Wo, Y. Li, S. Shen, B. Pan, Q. Wang, H. C. Walker, P. Steffens, M. Boehm, Y. Hao, D. L. Quintero-Castro, L. W. Harriger, M. D. Frontzek, L. Hao, S. Meng, Q. Zhang, G. Chen, and J. Zhao, *Nature (London)* **540**, 559 (2016).
- [10] J. A. M. Paddison, M. Daum, Z. Dun, G. Ehlers, Y. Liu, M. B. Stone, H. Zhou, and M. Mourigal, *Nat. Phys.* **13**, 117 (2017).
- [11] Z. Zhu, P. A. Maksimov, S. R. White, and A. L. Chernyshev, *Phys. Rev. Lett.* **119**, 157201 (2017).
- [12] M. Majumder, G. Simutis, I. E. Collings, J.-C. Orain, T. Dey, Y. Li, P. Gegenwart, and A. A. Tsirlin, *Phys. Rev. Research* **2**, 023191 (2020).
- [13] J. Iaconis, C. Liu, G. B. Halász, and L. Balents, *SciPost Phys.* **4**, 003 (2018).
- [14] Y.-D. Li, Y.-M. Lu, and G. Chen, *Phys. Rev. B* **96**, 054445 (2017).
- [15] Z. Ma, J. Wang, Z.-Y. Dong, J. Zhang, S. Li, S.-H. Zheng, Y. Yu, W. Wang, L. Che, K. Ran, S. Bao, Z. Cai, P. Cermak, A. Schneidewind, S. Yano, J. S. Gardner, X. Lu, S.-L. Yu, J.-M. Liu, S. Li *et al.*, *Phys. Rev. Lett.* **120**, 087201 (2018).
- [16] Y. Li, S. Bachus, B. Liu, I. Radelytskyi, A. Bertin, A. Schneidewind, Y. Tokiwa, A. A. Tsirlin, and P. Gegenwart, *Phys. Rev. Lett.* **122**, 137201 (2019).
- [17] *Muon Spectroscopy: An Introduction*, edited by S. J. Blundell, R. De Renzi, T. Lancaster, and F. L. Pratt (Oxford University Press, Oxford, 2021).
- [18] W. Steinhart, P. A. Maksimov, S. Dissanayake, S. Shi, N. P. Butch, D. Graf, A. Podlesnyak, Y. Liu, Y. Zhao, G. Xu, J. W. Lynn, C. Marjerrison, A. L. Chernyshev, and S. Haravifard, *npj Quantum Mater.* **6**, 78 (2021).
- [19] F. L. Pratt, S. J. Blundell, T. Lancaster, C. Baines, and S. Takagi, *Phys. Rev. Lett.* **96**, 247203 (2006).
- [20] F. Xiao, J. S. Moller, T. Lancaster, R. C. Williams, F. L. Pratt, S. J. Blundell, D. Ceresoli, A. M. Barton, and J. L. Manson, *Phys. Rev. B* **91**, 144417 (2015).
- [21] M. Takigawa, N. Motoyama, H. Eisaki, and S. Uchida, *Phys. Rev. Lett.* **76**, 4612 (1996).
- [22] S. Guchhait, Q.-P. Ding, M. Sahoo, A. Giri, S. Maji, Y. Furukawa, and R. Nath, *Phys. Rev. B* **103**, 224415 (2021).

- [23] S. Mañas-Valero, B. M. Huddart, T. Lancaster, E. Coronado, and F. L. Pratt, *npj Quantum Mater.* **6**, 69 (2021).
- [24] B. Bertini, F. Heidrich-Meisner, C. Karrasch, T. Prosen, R. Steinigeweg, and M. Žnidarič, *Rev. Mod. Phys.* **93**, 025003 (2021).
- [25] M. Ljubotina, M. Žnidarič, and T. Prosen, *Nat. Commun.* **8**, 16117 (2017).
- [26] T. Lancaster, P. J. Baker, F. L. Pratt, S. J. Blundell, W. Hayes, and D. Prabhakaran, *Phys. Rev. B* **85**, 184404 (2012).
- [27] B. M. Huddart, M. Gomilsek, T. J. Hicken, F. L. Pratt, S. J. Blundell, P. A. Goddard, S. J. Kaech, J. L. Manson, and T. Lancaster, *Phys. Rev. B* **103**, L060405 (2021).
- [28] Muon data from this study is available from the ISIS Facility: <https://doi.org/10.5286/ISIS.E.RB1920344>.
- [29] See Supplemental Material at <http://link.aps.org/supplemental/10.1103/PhysRevB.106.L060401> for further information about the muon site and its coupling to the electronic spins.
- [30] See Supplemental Material at <http://link.aps.org/supplemental/10.1103/PhysRevB.106.L060401> for detailed information about the β parameter.
- [31] See Supplemental Material at <http://link.aps.org/supplemental/10.1103/PhysRevB.106.L060401> for some more detailed plots of the LF dependence of the polarization function and the relaxation rate.
- [32] F. Devreux, J-P. Boucher, and M. Nechtschein, *J. Phys. France* **35**, 271 (1974).
- [33] M. A. Butler, L. R. Walker, and Z. G. Soos, *J. Chem. Phys.* **64**, 3592 (1976).
- [34] See Supplemental Material at <http://link.aps.org/supplemental/10.1103/PhysRevB.106.L060401> for analysis of the LF dependent relaxation rate in YMGO.
- [35] T. Moriya, *Prog. Theor. Phys.* **16**, 23 (1956).
- [36] S. J. Clark, M. D. Segall, C. J. Pickard, P. J. Hasnip, M. J. Probert, K. Refson, and M. C. Payne, *Z. Kristallogr.* **220**, 567 (2005).
- [37] J. P. Perdew, K. Burke, and M. Ernzerhof, *Phys. Rev. Lett.* **77**, 3865 (1996).
- [38] P. M. Chaikin and T. C. Lubensky, *Principles of Condensed Matter Physics* (Cambridge University Press, Cambridge, 1995).
- [39] F. Verstraete, M. Popp, and J. I. Cirac, *Phys. Rev. Lett.* **92**, 027901 (2004).
- [40] P. Hauke, M. Heyl, L. Tagliacozzo, and P. Zoller, *Nat. Phys.* **12**, 778 (2016).
- [41] P. Laurell, A. Scheie, C. J. Mukherjee, M. M. Koza, M. Enderle, Z. Tylczynski, S. Okamoto, R. Coldea, D. A. Tennant, and G. Alvarez, *Phys. Rev. Lett.* **127**, 037201 (2021).
- [42] Y. Xu, J. Zhang, Y. S. Li, Y. J. Yu, X. C. Hong, Q. M. Zhang, and S. Y. Li, *Phys. Rev. Lett.* **117**, 267202 (2016).
- [43] C. P. Nave and P. A. Lee, *Phys. Rev. B* **76**, 235124 (2007).
- [44] M. Yamashita, N. Nakata, Y. Senshu, M. Nagata, H. M. Yamamoto, R. Kato, and Y. Matsuda, *Science* **328**, 1246 (2010).
- [45] P. Bourgeois-Hope, F. Laliberté, E. Lefrançois, G. Grissonnanche, S. R. de Cotret, R. Gordon, S. Kitou, H. Sawa, H. Cui, R. Kato, L. Taillefer, and N. Doiron-Leyraud, *Phys. Rev. X* **9**, 041051 (2019).
- [46] J. M. Ni, B. L. Pan, B. Q. Song, Y. Y. Huang, J. Y. Zeng, Y. J. Yu, E. J. Cheng, L. S. Wang, D. Z. Dai, R. Kato, and S. Y. Li, *Phys. Rev. Lett.* **123**, 247204 (2019).
- [47] M. Yamashita, *J. Phys. Soc. Jpn.* **88**, 083702 (2019).
- [48] R. Kato, M. Uebe, S. Fujiyama, and H. Cui, *Crystals* **12**, 102 (2022).
- [49] R. V. Mishmash, J. R. Garrison, S. Bieri, and C. Xu, *Phys. Rev. Lett.* **111**, 157203 (2013).